ILASS 2008
Sep. 8-10, 2008, Como Lake, Italy

Paper ID ILASS08-6-2

NUMERICAL AND EXPERIMENTAL INVESTIGATION OF FUEL INJECTION AND DROPLET EVAPORATION IN A PRESSURE CHAMBER FOR THE DEVELOPMENT OF GASOLINE DIRECT INJECTION

Junmei Shi*[1], Harald Baecker*, Milos Tichy*, Wolfgang Bauer°

* Continental Automotive GmbH, Siemensstr. 12, D-93055 Regensburg
[1] Tel.49-941-790-8223, email: Junmei.Shi@continental-corporation.com
° ANSYS Germany GmbH, Staudenfeldweg 12, D-83624 Otterfing

ABSTRACT
This work deals with the spray behaviour of a PDI injector for gasoline fuel, which is driven by a piezoelectric element and equipped with a outward opening A-shape hollow cone valve. Spray characterization experiments were carried out in a conditioned pressure chamber by using Mie scattering technique and PDA measurement. First, the experiment was performed for non-evaporating spray by keeping the chamber temperature at 20 °C and fuel temperature at -10 °C. Spray contour, droplet size and velocity were obtained for various rail and chamber pressure values. Then the Mie scattering technique was applied to characterize evaporating sprays under equivalent engine operation conditions. Fuel variation was performed for n-hexane, isooctane, n-decane, fuel mixtures consisting of n-hexane, isooctane and n-decane, ethanol, gasoline and E85. The data obtained were used for the validation of the simulation results. The CFD simulation was based on the Lagrange approach using the commercial code ANSYS CFX11. Calibration was carried out for the Cascade Atomization and drop Breakup (CAB) model by using the PDA measurement and the Mie spray images. The combined experimental and numerical investigation provided detailed understanding of the fuel injection process and the spray behaviour.

INTRODUCTION

The modern gasoline direct-injection (GDI) engine adopting the spray-guided and stratified combustion strategy offers many advantages in terms of fuel economy, efficiency and exhaust emission reduction. The spray-guided combustion technique mainly utilizes the flow dynamic of the injection process to achieve suitable fuel vapour-air mixture for ignition and combustion. The PDI injector developed for gasoline direct injection engine provides new potential in promoting the GDI technology. Thanks the high switching speed of the piezoelectric actuator and the high injection pressure, multiple injections with a very short injection interval and a dramatically reduced minimum injection mass level can be realized. In addition, the actuation energy is tuneable allowing the control of needle lift and thus further increases the flexibility of injection realization. Enhanced with the A-shape cone valve (see Fig. 1), the PDI spray cone is very stable, mainly determined by the valve geometry but almost independent on the chamber pressure during the injection time. Through injection and ignition timing control, optimal stratified fuel-gas mixture can be achieved under a wide range of engine operating conditions [1].

One fundamental issue of stratified combustion optimization is to understand the physical phenomena occurring in the fuel injection and mixture preparation phase, namely atomization, droplet evaporation, the spray-induced vortex structure and mixing [2]. Due to the complex nature of these physical processes, engineering spray simulation has to rely on a number of empirical models [3]. Hence, it is necessary to do careful model validation. In this work, extensive spray characterization was carried out using various single and multiple component fuels in order to establish experimental database for spray model validation. The numerical investigation was focused on the non-evaporating spray, because no-quantitative reference data were available for the evaporation. The secondary breakup model was calibrated against the PDA measurement results and the spray visualization images. The numerical results also provided a deep understanding of the experimental observations

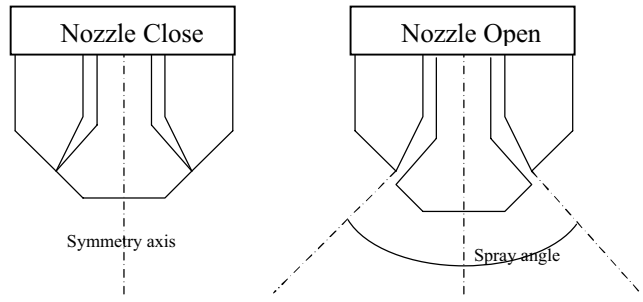

Fig. 1: Schematic of A-shape outward-opening cone valve

EXPERIMENTAL SPRAY CHARACTERIZATION

Spray characterization was carried out in a conditioned pressure chamber using Mie light scattering visualization and LDA/PDA measurement. The fuel was cooled or pre-heated with three tube-in-tube heat-exchangers. To reduce fluctuations of the fuel pressure during the injection process a pressure reservoir was installed in front of the injector. To minimize heat losses between the heat-exchangers and the injector, the tubes and the pressure reservoir were

additionally surrounded with a flexible conditioning tube and isolation material.

Experimental setup

The experiment setup for Mie light scattering spray visualization is schematically illustrated in Fig. 2. Two flash lamps were used for illumination. The scattered light was detected under 90° using a CCD camera. At each trigger delay 32 images were taken. Camera, flash lamps and injector were synchronized with an external trigger unit. The CCD camera has a resolution of 1280x1024 pixels. The resulting local resolution is 127.1 µm/pixel for the Mie integral images.

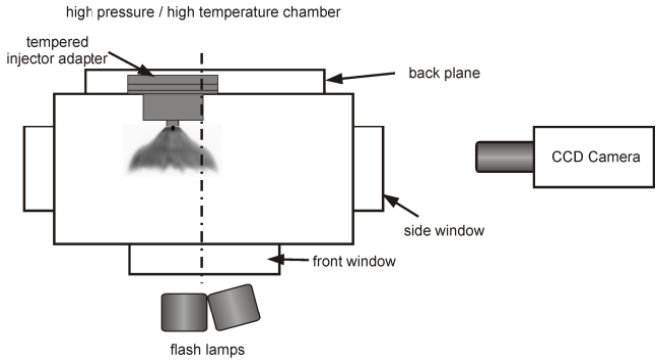

Fig. 2: Experimental setup of Mie spray visualization.

Droplet size and droplet velocities were measured using the Laser Doppler (LDA) / phase Doppler anemometry (PDA). For the determination of the LDA/PDA-measurement positions, the radial Mie-scattering light sheet technique was first applied to visualize the thickness of the spray. The setup is shown in Fig. 3.

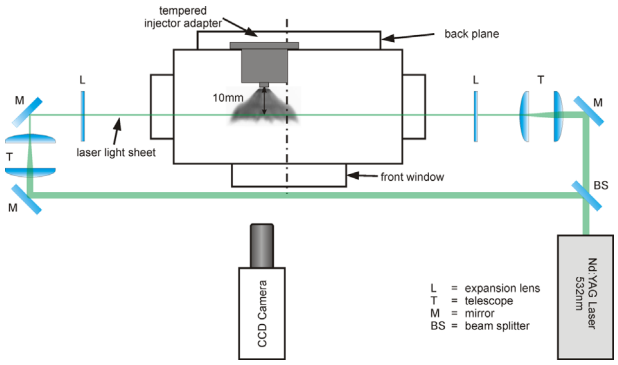

Fig. 3: Experimental setup of Mie-scattering light sheet

For the visualization of the radial spray structures the beam of a frequency-doubled, pulsed Nd: YAG-Laser (532 nm) was formed to a thin light sheet of 0.5 mm thickness at 10 mm from the spray cone origin by a system of cylindrical lenses. To minimize effects of extinction within the spray, the light sheet is coupled simultaneously into a test chamber from both sides. The light scattered by the fuel droplets was detected perpendicularly to the measurement plane with a CCD camera. Again, each average image was obtained from 32 image shots. The local resolution of the radial image is 73.8 µm/pixel.

The setup of Laser Doppler (LDA) / phase Doppler anemometry (PDA) measurement is displayed in Fig. 4 and the measurement locations in Fig. 5. A commercially available Particle Dynamics Analysis system was used. The beam of an argon ion laser was split up and utilized for the Doppler interferometry. The laser beams, one of them shifted in frequency by 40 MHz, were overlapped in an intersection volume by transmitter optics using a 310 mm collimator lens. The resulting probe volume was 1 mm in length with a diameter of 73 • m. The probe volume was positioned within the spray field with an accuracy of smaller than 0.01 % using a 3-stage traversing unit. The detection angle was chosen to be 69° in order to minimize the influence of a possible refractive index change due to temperature changes (Brewster angle). The signal bursts were detected with an optical receiver using a lens with a focal length of 300 mm and the receiving aperture mask for small particles. The tolerance band for spherical validation of the droplet size was preset in the recording software to 10%.

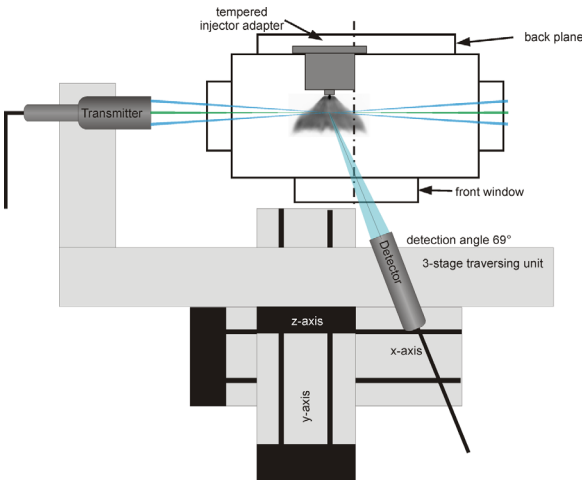

Fig. 4: PDA measurement setup

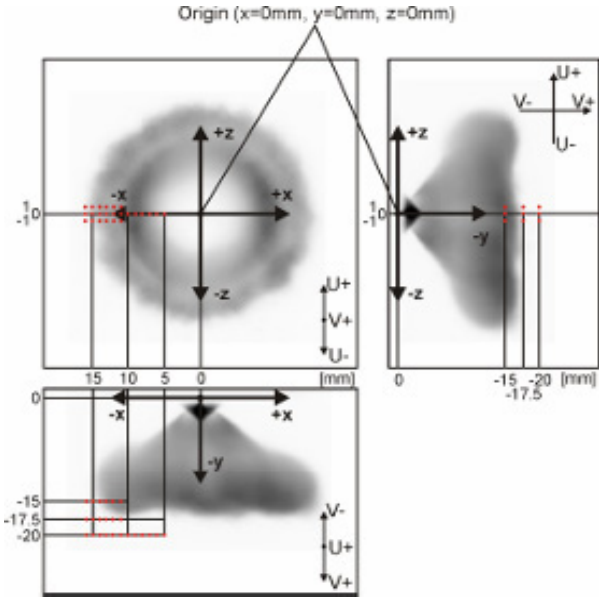

Fig. 5: Coordinate system of PDA measurement

The experiments were respectively conducted for "non-evaporating" spray and realistic spray in order to isolate the evaporation effect from the atomization process. The measurement for the so-called "non-evaporating" spray was

performed at the chamber temperature of 20 °C and the gasoline fuel temperature at -10 °C, so as to keep the evaporation negligible. Both Mie scattering and PDA were applied for the cold spray experiment. For the evaporating spray characterization, the pressure and temperature of the fuel and chamber were adjusted to the values equivalent to the realistic engine operation conditions. The experiment was conducted for various fuels include n-hexane, isooctane, n-decane, ethanol, gasoline and E85 (85% ethanol, 15% gasoline). The investigation was mainly based on the Mie scattering technique. From the Mie images, the spray-induced vortex structure, the penetration, and the spray evaporation time can be obtained. The experimental results provide useful reference for simulation validation. The laser-induced fluorescence (LIF) measurement technique was also tried to visualize the vapour distribution. Nevertheless, it was found that the calibration problem of LIF measurement in a chamber has first to be solved, which is much more difficult than the calibration in a glass engine.

Non-evaporating spray

In the non-evaporating spray experiments the rail and chamber pressure were varied. The operation conditions of some test cases are given in Table 1. The cases OP01 and 02 correspond to stratified combustion operation mode at full and partial loads, respectively. OP03 corresponds to homogeneous combustion mode. The injection pulse was fixed to 0.4 ms for all cases.

Table 1: Test cases for cold spray characterization

OP	T fuel	P rail	P chamber	T chamber	Injection time
	[°C]	[bar]	[bar]	[°C]	[ms]
01	-10	200	15	20	0.4
02	-10	100	15	20	0.4
03	-10	100	1	20	0.4

Mie integral and radial light sheet images were obtained at every 50 μs time interval after the visible injection. At each trigger delay 32 shots were taken. The averaged spray images for the time instant 0.5 ms after the visible injection are displayed in Figs. 6-7. In all cases, almost axially symmetrical fuel sprays around the injector axis were observed. Very compact sprays with strong recirculation zones at the propagation front can be observed in the test cases OP01 and OP02, where the chamber pressure is 15 bar. This is an advantageous feature of the PDI spray over the conventional multi-stream spray for stratified combustion, as well as for the spark ignition. In contrast, a perfect cone spray with uniformly distributed streaks is observed in test case OP03. The penetration is also much larger for the low chamber pressure.

The spray-induced recirculation (vortex structure) is observed right after the visible injection (t = 0.1 ms, not shown here). The vortex structure increases and moves downstream with the spray propagation. Large vortex structures appear after the injection time. It is interesting to note from the visualizations demonstrated in Fig 8 that the spray seems to move to the cone centre through recirculation and propagates downstream along the injector axis. The radial light sheet images of Fig. 9 also support this observation. The flow pattern together with the instant spray contours and their dependence on the operating conditions is an important feature for spray characterization. It is difficult to get a clear picture of the spray distribution purely from the Mie integral images. CFD simulation will be useful to obtain detailed information of the vortex structure and a clear understanding of the spray propagation and recirculation process.

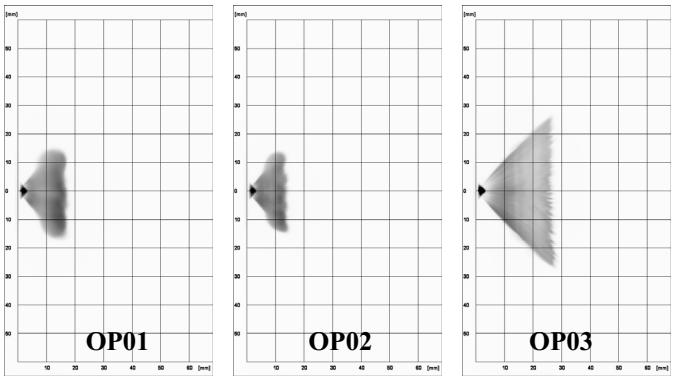

Fig. 6: Integral Mie images at t =0.5 ms

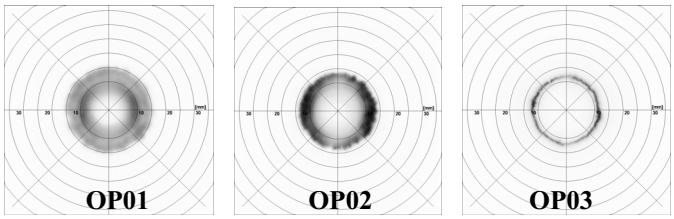

Fig. 7: Radial Mie light sheet images at t =0.5 ms

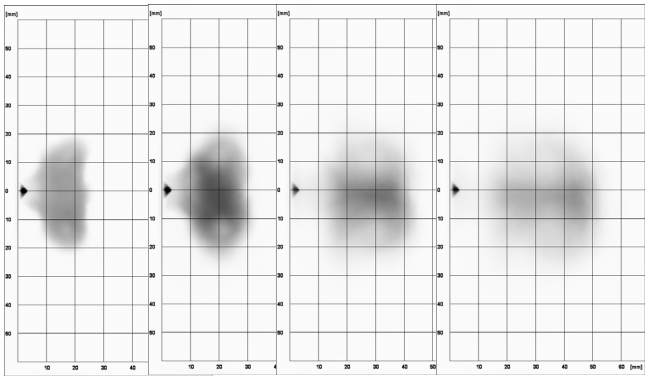

Fig. 8: Integral Mie images at t = 1, 2, 6, 10 ms, OP01

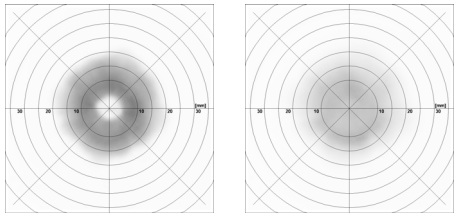

Fig. 9: Radial Mie light sheet images at t =1, 2 ms, OP01

Spray under engine operating conditions

The spray characterization under realistic engine operation conditions was aimed at producing reference data for CFD evaporation model validation. In the experiment the

rail pressure, fuel temperature, and the gas pressure and temperature in the chamber were adjusted to the equivalent engine operating conditions. Spray visualization experiment was carried out using the following single component fuels and their mixtures: n-hexane (high volatility), isooctane (middle volatility), n-decane (low volatility), a two-component fuel mixture denoted by mixture2 (72.05% n-hexane, 27.95% n-decane) and a three-component fuel mixture denoted by mixture3 (35% n-hexane, 45% isooctane, 20% n-decane). The composition of the fuel mixture is defined such that the boiling point matches the middle point of the normal gasoline fuel boiling curve in order to examine their capability of being used as model fuel to represent the real gasoline fuel for numerical simulation. In addition, experiment was also performed for normal gasoline fuel, ethanol and E85. Some spray visualization results under the stratified full load operation condition are displayed in Figs. 10-11, where P_{rail} = 200 bar, T_{fuel} = 70 °C, $P_{chamber}$ = 15 bar, and $T_{chamber}$ = 200 °C. The injection time is 0.225 ms for all cases. No visualization is presented for the n-hexane spray in Fig. 11, since the spray is almost not visible at t=1 ms after the injection start for its fast evaporation process. It can be confirmed that the evaporation rate of the three-component mixture fuel spray is close to but slightly faster than the real gasoline spray among all cases. In contrast, the isooctane spray evaporates much faster than the normal gasoline spray. Therefore, it is not optimal to use isooctane as the model fuel to represent the gasoline fuel, which is nevertheless a common practice in many industrial simulations of mixture formation. In addition, it is surprising that the evaporation rate of the two-component fuel mixture sprays with 27.95% n-decane mass fraction seems higher than the three-component fuel spray with only 20% mass fraction of n-decane. This might be mainly due to the much higher vapor pressure of mixture2 than that of the mixture3. Therefore, in addition to the boiling point, the effective vapor pressure and also other thermo physical properties need to be considered as further criterion for the definition of the model fuel.

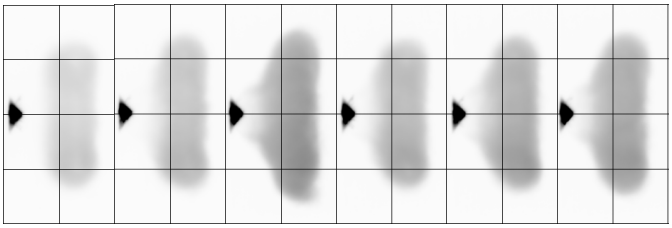

n-hexane isooctane n-decane mixture2 mixture3 gasoline

Fig. 10: Mie integral images of various fuel sprays, t = 0.5 ms

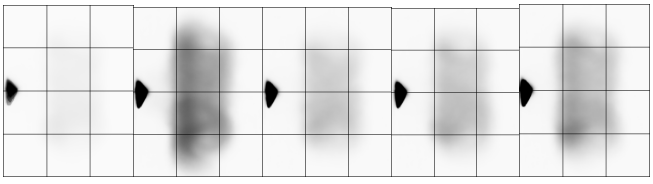

isooctane n-decane mixture2 mixture3 gasoline

Fig. 11: Mie integral images of various fuel sprays, t = 1 ms

NUMERICAL INVESTIGATION

Considering the fact that no quantitative reference data (LIF) was available for the evaporation model validation, the numerical investigation was limited to the non-evaporating spray with a focus on the secondary breakup model calibration.

In a previous work [4] model evaluation was carried out for the secondary breakup models based on the Rayleigh-Taylor instability theory available in the commercial code ANSYS CFX11, namely the Taylor Analogy Breakup (TAB) model [5], the Enhanced TAB model (ETAB) and the Cascade Atomization and drop Breakup (CAB) model by Tanner [6-7]. The evaluation was based on the spray penetration length and the spray outer contour obtained from the Mie scattering experiment. It was found that the TAB model produces too small droplets and thus much reduced penetration. Among these three models the CAB model performs the best in most of the test cases. One exception is the case with P_{rail}= 100 bar, $P_{chamber}$= 1 bar, where the Weber number based on the droplet diameter was about We= 262.

Recently, similar observation was also reported in [8] for the multi-stream spray. In that work the authors proposed a correlation function depending on the injection Weber number for the bag breakup regime model constant in order to make the CAB model applicable to a wide range of Weber numbers. It is assumed in the CAB model that the rate of child droplets generation is proportional to the number of child droplets:

$$\frac{d}{dt}n(t) = 3K_{br}n(t) \quad (1)$$

The breakup frequency depends on the breakup regime (bag, stripping or catastrophic) and is given by:

$$K_{br} = \begin{cases} k_1\omega & 5 < We < We_{t1} \\ k_2\omega\sqrt{We} & We_{t1} < We < We_{t2} \\ k_3\omega We^{3/4} & We_{t2} < We \end{cases}, \quad (2)$$

where • is the drop oscillation frequency defined as in the TAB model, *We* is the Weber number based on the droplet radius.

The bag breakup regime constant k_1 = 0.05 in the standard CAB model was determined to match the experimental data, whereas the values for the constants k_2 and k_3 were chosen to provide continuous K_{br} at the regime-dividing Weber numbers, We_{t1} and We_{t2}. In [8] a correlation as a function of the Weber number was introduced for the bag breakup regime model constant k_1. The correlation function was obtained from extensive model calibration based on PDA measurement of sprays produced by multi-stream atomizers.

The novel PDI injector dealt with here has a very different feature from multi-stream atomizer. The present numerical study was intended to obtain calibration for the CAB model constant k_1 for various operation conditions by taking advantage of the PDA measurement and spray visualization results aimed at developing a predictive spray simulation approach. Another aim was to understand the spray-induced flow pattern observed in spray visualization experiment.

Numerical method and simulation set up

The numerical simulation was based on the Lagrange approach using the commercial code ANSYS CFX11 [9]. For the Euler phase, a three-dimensional Navier-Stokes solver based on an element-based finite volume method using collocated variable arrangement on unstructured grids is available. The gas phase flow is described by the Reynolds averaged conservation equations for mass, momentum using the k-epsilon turbulence model. A high resolution discretization scheme was used for the convective terms and a second order backward Euler scheme for the time discretization in order to obtain a second order error reduction in space and time.

The particle tracking module was applied for tracking the motion of the spray droplets. The effects of droplet breakup, turbulence dispersion, and momentum exchange with the gas phase based on Schiller-Naumann drag correlation were considered. The influence of the droplets on the continuous phase is modeled via a momentum source term in the gas phase equations. The effect of streak formation and primary breakup were neglected.

The computation was performed using a three-degree sector mesh with one cell in the circumferential direction based on the assumption that the flow is axis-symmetrical corresponding to the injector axis. The computational domain is 140 mm in the axial (z) and 100 mm in the radial (y) direction. The core part of the mesh is displayed in Fig. 12. Around the spray cone grid refinement was applied in order to achieve sufficient resolution in the shear layer induced by the fuel injection. The smallest mesh edge size is 16 µm.

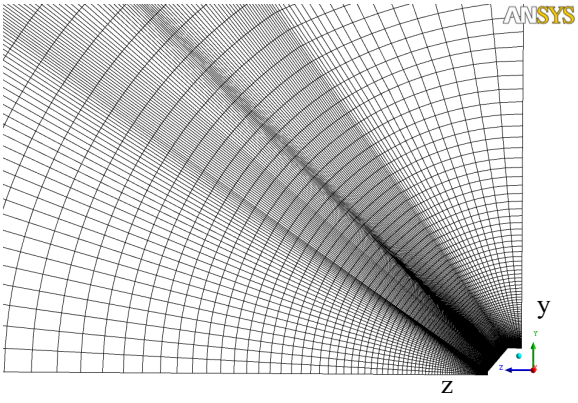

Fig. 12: The computational grid close to injector

The operating points are listed in Table 1. The injection velocity was estimated from the following equation:

$$U = C\sqrt{2\,dp/\rho_l} \qquad (3)$$

where C is the discharge coefficient, dp is the pressure difference between rail and chamber, and ρ_l the fuel density. Since the discharge coefficient is unknown, values from 0.75 to 0.9 were tested to match the experimental results. The injection mass was determined from experiment. In order to taking into account of the transient effect related to the needle opening and closing, the injection mass flow rate was assumed to be linear to the needle lift.

For the particle tracking computation, the isooctane fuel was applied as model fuel. The surface tension coefficient under the operation conditions -10 °C is 0.02117 N/m. For each computation, at least 6500 parcels were tracked. At each time step the number of the parcels entered in the computational domain was set to be proportional to the instant injection mass flow rate.

In order to ensure the numerical accuracy, numerical experiments were carried out to gain best practice guides for the computational grid and numerical parameters. Effects of the numerical parameters, e.g. grid size, time step, iteration number, number of coefficient loops, and number of tracking parcels etc., on the numerical results were investigated. Computation was also carried out using a 15 ° sector domain with 5 cells in the circumferential direction. No essential difference in flow pattern, penetration and spray distribution was found.

Test case OP01

For the calibration of the CAB model, the value of the bag breakup regime constant k_1 was varied between 0.01 and 0.05. Numerical experiment was also performed by varying the initial droplet diameter and the injection velocity. The same as in the PDA measurement experiment, the droplet size distribution was evaluated for various locations within a time interval of 3 ms after the injection start. The simulation results were compared with the PDA measurement data. The results for the location y = -15 mm and x = -15 mm in the PDA measurement coordinate system (refer to Fig. 5), which corresponds to z=15 mm and y = 15 mm here (refer to Fig. 12), is presented in Fig. 13, where the size distribution was calculated by using a size class bin 2µm. In addition to k_1, the initial droplet diameter D_0 and the injection velocity U are also specified. These results confirm the finding of [8] that the model constant k_1 has a significant effect on the droplet size distribution. The predicted droplet size is much too small by using the default value $k_1 = 0.05$. Refer to eq. (1) and (2), the breakup process can be slow down by reducing k_1. A fairly good match to the PDA measurement was obtained by using k_1 = 0.01 in combination with D_0 = 100 µm and an injection velocity U = 180 or 200 m/s. Nevertheless, in both cases, the predicted spray distribution and the flow pattern deviate too much from the Mie spray visualization. This might be due to the limitation of the PDA measurement, which is discussed below.

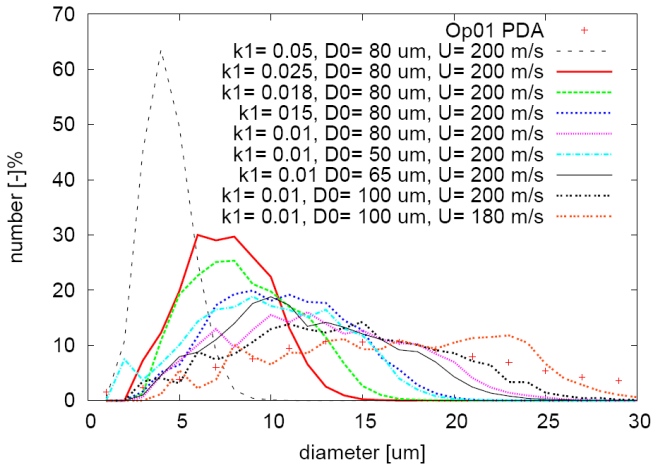

Fig. 13: Comparison of predicted and measured droplet diameter distribution, y = -15 mm and x = -15 mm (refer to Fig. 5), which corresponds to z=15 mm and y = 15 mm here (refer to Fig. 12).

Results from time-resolved analysis of the PDA data are displayed in Fig. 14. The main data collection occurred during two time intervals, t = 0.5 – 0.75 ms and t = 1 – 3 ms. It can be recognized that the first interval corresponds to the needle opening phase, where the mean value of the droplet velocity component along the injector axis *v* is up to 20 m/s. In this time interval the mean droplet diameter D10 is about 15 µm. Only a few valid signals were collected during the main body injection, probably due to high spray density. The main fraction of the samples was collected during the second time interval from the droplets transported by the flow recirculation, where the velocity component *v* almost decreases to zero. It is interesting to note that the mean droplet diameter D10 increases from 10 µm to about 20 µm during the second interval. Therefore, the present PDA measurement might probably overestimate the droplet size.

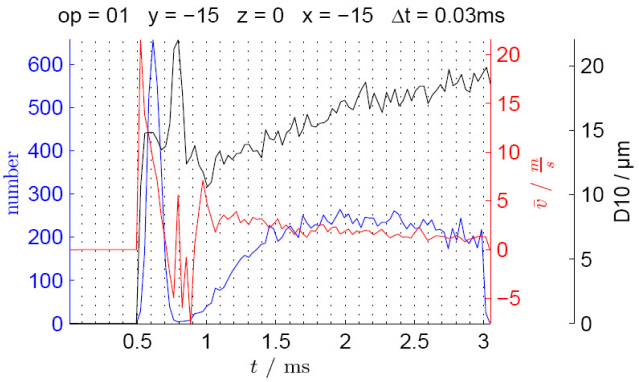

Fig. 14: Time series of signal number, mean droplet diameter D10, and the velocity component along the injector axis calculated from the PDA data.

Another important criterion for the model calibration is the spray distribution and the fuel-injection induced flow pattern. For this purpose, numerical spray images were produced in the following way, first by making 60 rotating copies of the 3° sector model to form a 180° model and then by a projection in the *x*-direction (for coordinate systems refer to Fig. 12). Every three numerical droplets were visualized. The droplet size was not distinguished due to the limitation of the ANSYS CFX11 post processing tool, which does not have the functionality of particle size visualization in a mono-colour mode. It was found that the outer spray contour obtained by using the combination $k1 = 0.01$ with $D0 = 65$ µm and $U = 200$ m/s agrees fairly well with the Mie spray images, as is demonstrated in Fig. 15. Despite the CFX limitation in post processing, the recirculation vortices can be recognized from the plots for t = 4 and 6 ms.

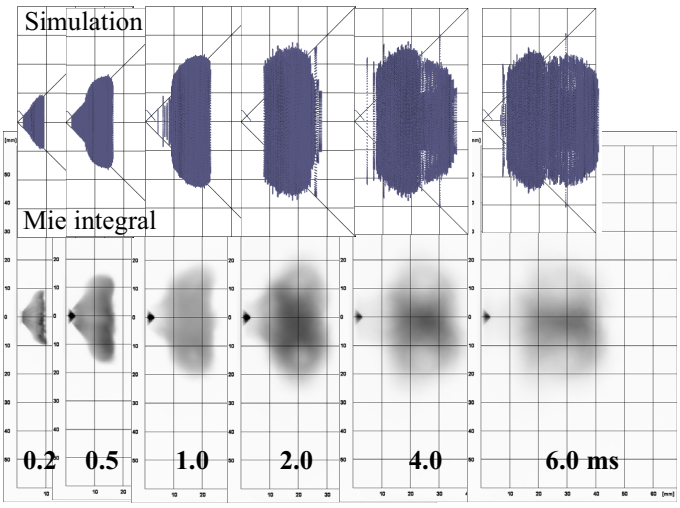

Fig. 15: Comparison of the spray outer contour.

In order to understand the physical cause for the formation of the vortex structure and the flow pattern, the evolution of the spray distribution over the 3° sector model over time is presented in Fig. 16. At t = 0.5 ms, a vortex pair along the spray cone can be observed. Further vortex pairs also exist in the downstream of the spray. It can be understood from the plots that the evolution of the upper vortex pair is responsible for the preferential concentration of the spray in the region around the injector axis at t = 4, 6 ms. The upper vortex pair occur right after the injection start, grow and move downstream along the spray cone with the time. The location of the vortex core inside the spray cone is higher that the counterpart outside the spray cone. There the pressure is lower than the corresponding outside region. However, the spray cone angle are very stable until t = 0.5 ms due to the high inertia of the spray coming from the injector. Thereafter the cone angle begins to decrease for the decreasing inertia of the spray from the injection due to the needle closing. This is

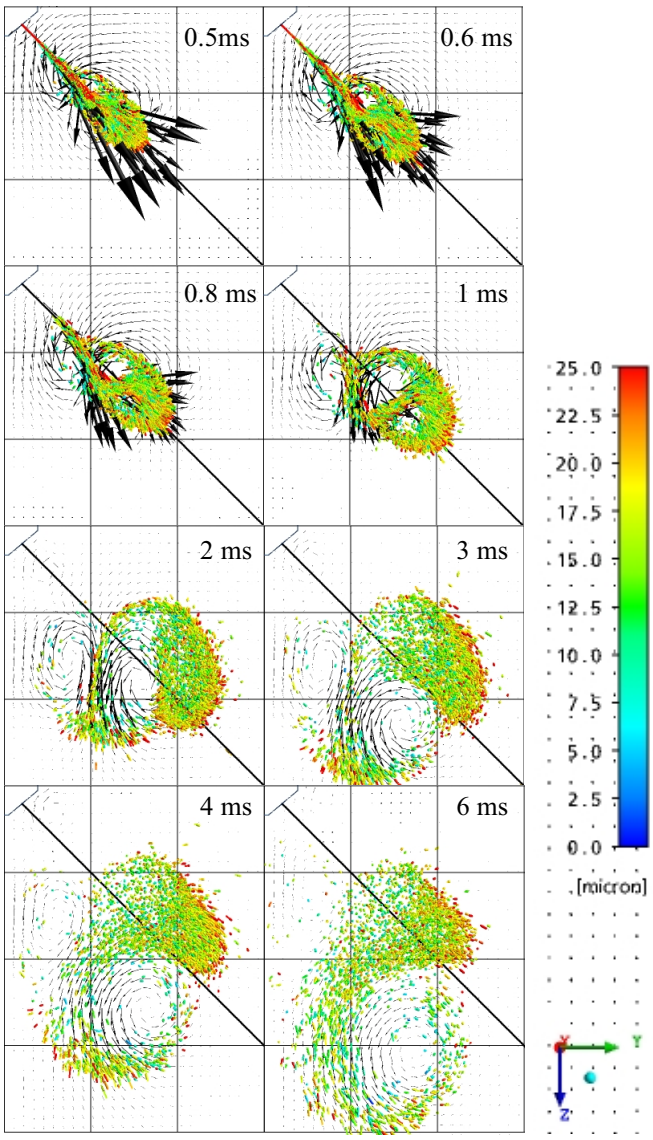

Fig. 16: Evolution of spray distribution over time, OP01.

shown for the time instant t = 0.6 ms. After the injection time, the air-entrainment induced recirculation outside of the spray cone pushes the inside vortex to move downwards and and enhances both vortices. This results in an anti-clock rotation of the vortex pair axis until t = 2 ms. In this process droplets, which are decelerated by the air drag, are entrained into the vortex motion with larger droplets in region between the two vortex cores and smaller droplets in the vortex cores. Between t = 2 and 3 ms, the interphase momentum exchange pushes the outside vortex to move downwards and the vortex pair start clockwise rotation. Finally the axis of the vortex pair becomes almost parallel to the original spray cone. As a result of this evolution process, the droplets are transported through the region between the vortex cores to the injector axis region.

Test case OP03

Model calibration was also carried out for the test case OP03 (Table 1). The results for the droplet size distribution at the PDA measurement location y = -15 mm and x = -15 mm (corresponding to z = 15mm, y = 15 mm in the numerical study) is presented in Fig. 17. The PDA results for the location x = -18 mm is additionally plotted. The computations based on k_1 = 0.5 agree fairly well with the measurement. The best match was obtained by the combination using k_1 = 0.5, D_0 = 80 µm, and an injection velocity U = 150 m/s. Therefore, the breakup process here is much faster than the case OP01. In contrast, the computation using the combination k_1 = 0.5 with D_0 = 60 µm, and U = 130 m/s produced best agreement with the spray contour from the Mie visualization. As an example, the results for t = 0.5 and 1 ms are demonstrated in Fig. 18. In the other cases using U = 150 m/s, the predicted spray propagation speed was found faster than that observed from the Mie visualization.

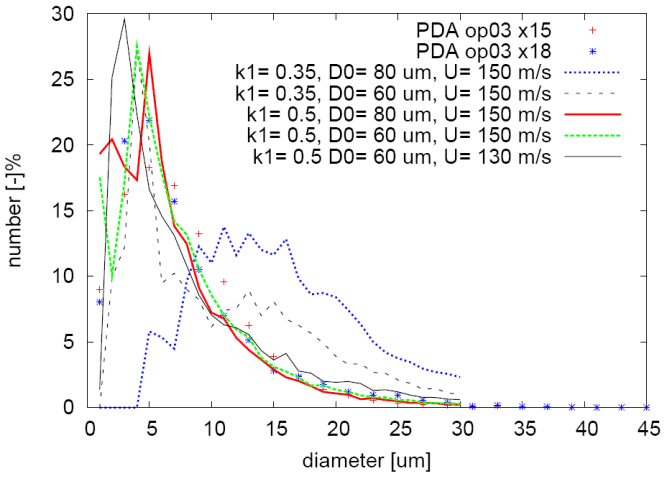

Fig. 17: Comparison of predicted and measured droplet diameter distribution, y = -15 mm and x = -15 mm (refer to Fig. 5), corresponding to z = 15mm, y = 15 mm in the numerical study (refer to Fig. 12)

Time series was also obtained from the PDA measurement data for the sample number, mean droplet diameter D10, and the velocity component v and are presented in Fig. 19. Different from the measurement of the case OP01, a big number of samples were collected during the main body injection. The measurement is easier in this case since the spray was much thinner due to the low chamber pressure, as can also be confirmed by the radial light sheet image shown in Fig.7. Since no essential recirculation is expected in this case, the number of signals decreases significantly shortly after the injection time. A small number of droplet samples were collected from the time interval 1 – 3 ms with a constant droplet size of about 5 µm and a low velocity decreasing with time. The simulation results displayed in Fig. 20 can confirm this observation. In addition, the simulation results also confirm the sinus motion of droplet reported in [10], which is caused by the spray induced vortices.

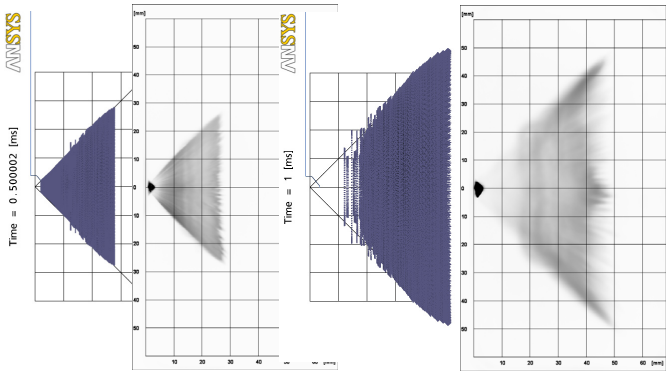

Fig. 18: Comparison of the spray outer contour, t = 0.5, 1 ms.

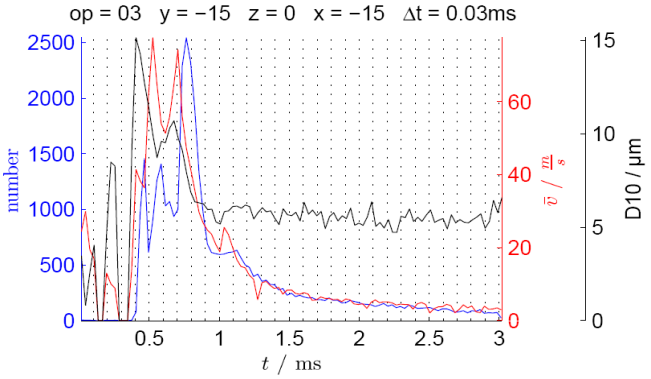

Fig. 19: Time series of signal number, mean droplet diameter D10, and the velocity component along the injector axis calculated from the PDA data.

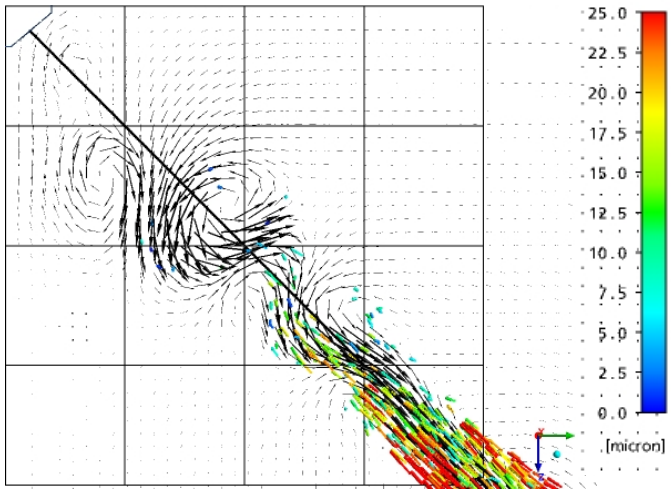

Fig. 19: Spray distribution, OP03, t = 1.5 ms.

CONCLUSION

In this work experimental and numerical investigation was carried out for the GDI spray of a PDI injector equipped with an outward opening A-shape hollow cone nozzle. Spray characterization experiments were carried out in a conditioned pressure chamber by using Mie scattering technique and PDA measurement. Fuel variation was performed for n-hexane, isooctane, n-decane, a two and three-component fuel mixture, ethanol, gasoline and E85. Data about droplet diameter and velocity distribution, spray propagation with time, and the flow pattern related to the spray induced recirculation were obtained. The experimental data obtained provided useful reference for the validation of the simulation results in order to develop predictive simulation approach. It was found that the evaporation rate of the isooctane fuel spray is much higher than the normal gasoline spray, and thus is not optimal as a model fuel for the GDI mixture formation simulation. In contrast, the evaporation behavior of the three-component mixture fuel consisting of n-hexane, isooctane, and n-decane was close to the normal gasoline fuel. The CFD simulation was based on the Lagrange approach using the commercial code ANSYS CFX11. Careful calibration was carried out for the Cascade Atomization and drop Breakup (CAB) model by using the PDA measurement and the Mie spray images. The numerical results confirmed the finding of [8] that the bag breakup regime model constant k_1 should be calibrated for different injection Weber number. It was found that k_1 = 0.01 is suitable for the case OP01 while k_1 = 0.5 is good for OP03. The numerical investigation also provides detailed flow field information for understanding the experimental observations.

ACKNOWLEDGMENT

The experimental spray characterization was carried out with the support of Esytech GmbH, Erlangen.

NOMENCLATURE

Symbol	Quantity	SI Unit
D10	Number Mean Diameter	
C	Discharge coefficient	
D_0	Initial Droplet Diameter	
K_{br}	Breakup Frequency	s^{-1}
P	Pressure	Pa
U	Injection velocity	m s^{-1}
T	Temperature	K
We	Weber number based on droplet radius	
We_{t1}	Critical Weber number of stripping breakup, = 80	
We_{t2}	Critical Weber number of catastrophic breakup, = 350	
dp	Pressure difference	Pa
k_1	CAB model breakup coefficient	
t	time	s
v	Velocity component	m
x	Coordinate component	m
y	Coordinate component	m
z	Coordinate component	
•	Drop oscillation frequency	s^{-1}
•	Density	kg m^{-3}

Subscripts

chamber	Chamber
rail	Rail
l	Liquid

REFERENCES

[1] H. Baecker, A. Kaufmann, M. Tichy, Experimental and Simulative Investigation on Stratification Potential of Spray-Guided GDI Combustion Systems, SAE2007-01-1407

[2] F.-Q. Zhao, M.-C. Lai, D. L. Harrington, A Review of mixture preparation and combustion control strategies for spark-ignited direct-injection gasoline engines, SAE970627

[3] W.A. Sirignano, Fluid Dynamics and Transport of Droplets and Sprays, Cambridge University Press, 1999.

[4] F. Vasquez, Numerical investigation of fuel atomization and evaporation in a pressure chamber for the development of gasoline direct injection, Master thesis, Technical University Berlin, March, 2008

[5] P.J.O'Rourke and A.A. Amsden, The TAB Method for Numerical Calculation of Spray Droplet Breakup, SAE Technical Paper, 872089, 1987.

[6] F.X., Tannner, Jet atomization and droplet breakup modeling of non-evaporating diesel fuel sprays. Int. J. of Heat and Mass Transfer, 106:127-140, 1998.

[7] F.X. Tannner, Cascade atomization and drop breakup model for the simulation of high-pressure liquid jets. SAE Paper 2003-01-1044, 2003.

[8] E. Kumzerova and T. Esch, Extension and validation of the CAB Droplet breakup model to a wide Weber number range, ILASS08-A132

[9] ANSYS, Inc.: ANSYS CFX-Solver Theory Guide, Release 11.0, 2006

[10] G. Wigley, PDA and CCD image analysis of three Siemens piezo GDI injectors, Siemens VDO internal report, 2004